

# **Simulation of overburden pressure during laboratory investigations of axial pipe-soil interaction**

B.B. Sheil, C.M. Martin and B.W. Byrne<sup>1</sup>

<sup>1</sup>Department of Engineering Science, University of Oxford, Parks Road, Oxford OX1 3PJ, UK

Original submission, 13 December 2018

Revised submission, 17 September 2019

Main text word count: 2452

Tables: 3

Figures: 10

## **ABSTRACT**

The simulation of additional soil overburden pressure through the use of a surcharge system is a technique commonly adopted in laboratory testing of pipe-soil interaction. This paper examines the role of surcharge boundary conditions and pressure level on the axial sliding behaviour of a trenched pipeline surrounded by sand backfill. A novel testing tank is employed in conjunction with a pressure bag system to simulate overburden pressure; both flexible and rigid surcharge boundary conditions are considered. Cyclic axial displacements are applied to a heavy pipe buried in a narrow trench, using two different sand backfills. The test pipe is instrumented to measure (a) the axial soil resistance developed on an isolated central section of pipe (thus avoiding tank boundary effects), and (b) the normal and shear contact stresses at a number of points around the pipe circumference. The results show that the type of surcharge boundary condition (flexible or rigid) has a significant influence on laboratory measurements of both the axial resistance and circumferential pressure distribution of a buried pipe section. Application and subsequent reduction of surcharge pressure is also shown to produce 'locked in' normal stresses on the pipe, thereby increasing the axial resistance. The results show that careful treatment of the surcharge boundary conditions and the surcharge pressure history are required to avoid unconservative predictions of field behaviour.

## INTRODUCTION

High pressure, high temperature (HPHT) pipelines experience frequent start-ups / shutdowns as well as diurnal temperature fluctuations, leading to complex packets of cyclic axial movements occurring along their length. These pipelines are commonly buried below ground for protection against mechanical damage but also to avail of the frictional restraint offered by the surrounding soil backfill. When designing for limit states, fatigue, buckling prevention, and economy, an accurate estimation of the axial soil restraint, and how it develops during cyclic axial movements, is essential.

The axial resistance of buried pipelines subjected to monotonic loading has been the subject of numerous investigations in the literature, e.g. Scarpelli et al. (2003), Anderson et al. (2004), Karimian (2006), Wijewickreme et al. (2009). By contrast, the role of cyclic axial movements has received much less attention and has largely been limited to experimental investigations involving flexible pipes, e.g. Weidlich and Achmus (2006), Bilgin and Stewart (2009), Huber and Wijewickreme (2014). A common feature of the vast majority of these experimental investigations is the use of a surcharge pressure system to simulate a greater depth of soil backfill than that actually present in the testing tank or trench. In general, two different methods feature in the literature: (i) a pressurized bladder reacting off a top plate, representing a flexible boundary condition, e.g. Höeg (1968), DiFrancesco et al. (1994), Rogers et al. (1996), Zanzinger and Gartung (1995, 1998), Brachman et al. (2000, 2001), Chapman et al. (2007); (ii) a rigid plate connected to a load-controlled hydraulic actuator, representing a rigid boundary condition, e.g. Kastner (1992), Sargand (1993), Kastner et al. (1993), Talesnick et al. (2011). Using finite element analysis, Brachman et al. (1996) noted that the latter set-up induces a complex stress regime around a buried pipe that is not necessarily representative of field conditions. However, to the authors' knowledge, no study has explicitly compared results derived using flexible and rigid surcharge boundary conditions.

The aim of this paper is to explore the role of surcharge boundary conditions and pressure level on laboratory measurements of axial pipe resistance. Selected results from a test programme carried out to support the design of a commercial onshore gas pipeline have been extracted for this purpose. Important features of the field project are discussed in Sheil et al. (2018) and include the narrow trench geometry, the heaviness of the pipe (due to a thick wall requirement for corrosion resistance), and the need to accommodate large-amplitude axial displacement cycles arising from thermal expansion and contraction.

## EXPERIMENTAL METHOD

### *Testing apparatus*

The testing discussed in this paper makes use of a new experimental apparatus designed specifically for investigating pipe-soil interaction at full scale (see Fig. 1; Sheil et al., 2018). A steel test pipe with outside diameter  $D = 0.35$  m was instrumented for measurement of the axial resistance developed on an isolated central section, in addition to ‘Stroud’ type load cells to measure the normal and shear contact stresses at a number of circumferential locations (see Fig. 2). In this study, the central pipe section was coated with Nap Gard 7-2610, a common epoxy coating used for steel oil and gas pipelines to provide improved corrosion resistance and mechanical durability. The Stroud cell lids were curved to ensure a flush finish with the pipe outer surface. The normal stresses measured by the Stroud cells are denoted  $\sigma_X$  where  $X$  is the location of the Stroud cell according to Fig. 2. The timber side walls of the soil tank (internal dimensions shown in Fig. 1) were left rough to mimic trench roughness in the field and were reinforced to ensure that lateral deflections during testing were  $< 1$  mm. The width of the tank was chosen to match the intended trench width of 0.95 m in the field project. The results presented in this paper focus on an effective pipe weight of 4 kN/m, reflecting the anticipated

self-weight of the pipe in the field project. Further information on the design and development of the experimental apparatus is available in Sheil et al. (2018).

#### *Test material and sample preparation*

Two candidate silty sand backfills for the field project were used in the testing; these are referred to as ‘Sand K’ and ‘Beach Sand’ henceforth (see Table 1). The processes adopted for sample preparation were developed to reflect likely practice at the field site. Vibratory compaction was carried out using a 400 mm × 320 mm commercial plate compactor on sand layers of 100 mm for 15 minutes each. Once the pipe had been laid down on a 300 mm compacted bed layer, no compaction was performed until the soil level was 100 mm above the pipe crown. This was to avoid damage to the fragile Stroud cells on the surface of the pipe.

#### *Simulation of overburden pressure*

The expected levels of soil overburden pressure in the field project were simulated using 0.35 m (i.e. one pipe diameter) of actual soil cover in conjunction with a pressure bag system. The pressure bag, which was connected to the laboratory compressed air supply via a regulator, reacted off a horizontal top plate (see Fig. 1) without interacting with the tank walls. Two different set-ups were adopted: (i) the pressure bag *below* a rigid wooden platen, i.e. a flexible surcharge boundary condition (Fig. 3(a)); (ii) the pressure bag *above* a rigid wooden platen, i.e. a rigid surcharge boundary condition (Fig. 3(b)). The effective nominal overburden pressure,  $\sigma'_v$ , acting at the level of the pipe crown was calculated as:

$$\sigma'_v = \gamma' h + p_{\text{bag}} A_r \quad (1)$$

where  $\gamma'$  is the effective unit weight of the soil (dry in these tests),  $h$  is the height of soil cover measured from the pipe *crown* (equal to 0.35 m in these tests),  $p_{\text{bag}}$  is the bag pressure and  $A_r$  is the pressure bag area ratio. For set-up (i), the full pressure in the bag is exerted onto the isolated central section of pipe due to the proximity of the bag to the pipe crown, and therefore

a value of 1 is adopted for  $A_r$  in Eq. 1. In the case of set-up (ii), the compressive force generated by the pressure bag is transferred to the soil via the timber platen, such that full spreading of the load is assumed to occur. Dividing the pressure bag plan area by the tank plan area gives  $A_r = 0.64$  to be used in Eq. 1.

#### *Testing procedure*

Table 2 summarises the tests discussed in this paper. Each test involved the application of displacement-controlled axial pipe movements, with alternating sets of large-amplitude cycles (20 mm) and small-amplitude cycles (2 mm), as shown in Table 3. The large-amplitude cycles represent pipe expansion / contraction due to pipeline start-up / shut-down, whereas the small-amplitude cycles correspond to diurnal temperature fluctuations. In the case of Test B1, additional cycles were appended to the main sequence to examine the role of surcharge pressure level on the adopted normalisation of axial resistance and the contact stress distribution (see Table 4).

## **EXPERIMENTAL RESULTS**

#### *Influence of surcharge boundary condition*

Figure 4 illustrates the influence of the surcharge boundary condition (flexible or rigid) on the development of normal contact stresses,  $\sigma'_n$ , around the pipe circumference during inflation of the pressure bag. Measured increases in  $\sigma'_n$  for each Stroud cell (locations given in Fig. 2) are plotted against the calculated increase in  $\sigma'_v$  ( $p_{\text{bag}} \times A_r$ ). Considering first the Sand K tests, the development of normal stress is generally a linear response to the increase in applied vertical pressure, as shown in Figs 4(a) and 4(b). Interestingly, an increase in the nominal overburden

pressure to ~3 kPa appears to transfer entirely to the (rough) walls of the soil tank. Both figures show that location S, the pipe invert, experiences the greatest increase in normal stress. This is consistent with previous experimental work on buried concrete pipes (Höeg, 1968). It can also be seen that the increases in  $\sigma_W$  and  $\sigma_E$  are much lower than would be expected from traditional lateral earth pressure calculations. One of the main reasons for this is the difficulty in compacting the sand around the sides of the pipe. Perhaps surprisingly, a flexible surcharge boundary induces a slightly greater increase in  $\sigma_N$  (Fig. 4(a)) than the rigid surcharge boundary (Fig. 4(b)). One major difference is evident in the Beach Sand tests, in comparison with the Sand K tests: the pressure increases measured at location S are significantly lower. This is due to minor longitudinal deviations in the level of the compacted bed layer, which have a significant influence on the values of  $\sigma_S$  developed in any given test.

Figure 5 shows the stress distributions before and after the cyclic axial testing, using polar plots of  $\sigma'_n/\sigma'_v$ . The radius at each location denotes the measured normal stress at that point,  $\sigma'_n$ , normalised by  $\sigma'_v$  where in this case  $\sigma'_v$  is the calculated vertical effective stress at the location of the corresponding Stroud load cell (i.e. the local embedment is used for  $h$  in Eq. 1). The plots show that the normal contact stresses are not symmetrical about the horizontal axis. Focusing on Tests K1 and K2, while the initial stress distributions are broadly similar (Fig. 5(a)), there is a marked difference between the two at the end of testing (Fig. 5(b)). Test K1 retains a similar shape, with slight increases in  $\sigma_{SE}/\sigma_{SW}$  and  $\sigma_N$ . In Test K2, there is a notable drop in  $\sigma_N$ , which is redistributed to locations NE/NW. This is due to the non-uniform vertical pressure exerted by the rigid platen on the sand as the pipe settles during testing (see Fig. 6). Similar findings may be deduced from the Beach Sand tests in Figs 5(c) and 5(d). It can also be seen that the two sand types exhibit broadly consistent behaviour.

Figure 7 plots the development of the measured peak axial resistance for each individual cycle during the cyclic axial testing. The axial resistance over the isolated central section,  $R_a$ , is

normalised by  $\sigma'_v \pi D$  where  $\sigma'_v$  is calculated (at the pipe crown) using Eq. 1. Differences in the ‘forward’ and ‘return’ normalised resistances for each cycle were minimal, so the average absolute normalised resistance for each cycle has been plotted against the number of large cycles. The packets of small-amplitude cycles are indicated with dashed vertical lines. Also superimposed on these plots are predictions determined using the ALA-ASCE (2001) design guidelines:

$$R_a = \gamma' H \cdot \frac{1 + K_0}{2} \cdot \tan \delta \cdot \pi D \quad (2)$$

where  $H$  is the depth of soil cover measured from the pipe *springline*,  $K_0$  is the coefficient of lateral earth pressure at rest for the soil and  $\delta$  is the pipe–soil interface friction angle. In accordance with ALA-ASCE (2001), the value of  $\delta$  is estimated as  $\delta = f\phi'$ , where  $\phi'$  is the friction angle of the backfill material and  $f$  is an interface strength reduction factor taken as 0.6 for the epoxy-coated central section of the test pipe (Sheil et al. 2018). On the basis of drained triaxial tests, critical state friction angles of  $31.1^\circ$  and  $30.9^\circ$  have been selected for Sand K and Beach Sand, respectively (see Table 1) and a value of 0.5 has been assumed for  $K_0$ . Figure 7(a) shows that the measured axial resistances were much higher in Test K2 than in Test K1. This is a result of confining the shear-induced soil dilation (occurring within the interface layer surrounding the pipe) with a rigid surcharge boundary (Fioravante et al., 1999, Porcino et al., 2003). There is, however, a general trend for the resistance to decrease with the number of cycles due to the inability of the rigid boundary condition to maintain a uniform distribution of vertical pressure as the pipe settles. In the case of the Beach Sand tests (Fig. 7(b)), the drop in axial resistance measured in the test with the rigid boundary (Test B2) is more pronounced. After only two cycles, resistance measurements for Test B2 drop below those observed in Test B1. It can be seen that the ALA-ASCE (2001) provides a poor prediction of the axial resistance as it does not consider the influence of pipe self-weight, which is significant for these tests.

Figure 8 confirms that greater pipe settlement occurs in the tests with a flexible boundary, with remarkably similar trends being evident between the two sand types.

#### *Influence of surcharge pressure level*

Additional cycles were appended to Test B1 to examine the influence of step changes in overburden pressure (through inflation of the pressure bag) on the peak axial resistance, averaged from the forward and return legs of each cycle as before. Figure 9 shows the variation of normalised axial resistance during the remaining large cycles, with vertical lines indicating adjustments in surcharge pressure. The high axial resistance measured for large cycle number 18 is due to densification during the preceding small-amplitude cycle set. Although an increase in *absolute* peak resistance was measured during the first cycle after each pressure increase phase (i.e. cycles 21, 24 and 27), Fig. 9 shows a significant but transient drop in *normalised* axial resistance. The normalised resistance subsequently returns to a ‘baseline value’ of ~0.52. This suggests that a certain amount of axial movement is required to fully mobilise the additional axial resistance developed in response to the increase in surcharge pressure. By contrast, although the *absolute* resistance decreases, the *normalised* resistance increases following a pressure decrease phase (cycles 30 – 32) and does not return to the ‘baseline value’. To investigate this further, the normal stresses around the pipe circumference at the end of cycles 20, 29 and 32 are plotted in Fig. 10. While the stress distribution measured in cycle 29 shows excellent agreement with the corresponding measurements for cycle 20, the results for cycle 32 are notably different. This indicates that a reduction in surcharge pressure appears to ‘lock in’ normal stresses on the pipe, particularly at the sides of the pipe. In light of this, design approaches derived from laboratory investigations may under-predict axial resistance in the field if the backfill soil is likely to have been preloaded.

186

## 187 **CONCLUSIONS**

188 The influence of surcharge boundary conditions and pressure level on the response of a buried  
189 steel pipe section subjected to cyclic axial displacements has been explored using a full-scale  
190 laboratory test rig. The results show that a rigid surcharge boundary condition yields higher  
191 measurements of the axial resistance initially, owing to the onerous confinement of the dilating  
192 soil cover. However, these resistances drop significantly as the pipe begins to settle, due to the  
193 non-uniform pressure distribution imposed by the rigid surcharge boundary. This contrasts with  
194 axial resistance measurements using a flexible surcharge boundary, which show slight  
195 increases during the cyclic axial testing. This suggests that experimental testing using a rigid  
196 surcharge boundary condition may under-predict long-term cyclic axial resistances that will be  
197 developed in the field. The tests also show that normalised peak resistances for axial  
198 displacement cycles undertaken following successive increases in surcharge pressure  
199 correspond very well, confirming the suitability of the traditional normalisation (by the nominal  
200 overburden pressure at the pipe crown) used in this paper. However, this normalisation does  
201 not hold following a subsequent reduction in surcharge pressure, which can be attributed to the  
202 presence of 'locked in' normal stresses around the sides of the pipe. It should be noted that the  
203 results presented in this paper pertain to a specific pipe / trench geometry and further  
204 experimental and / or numerical investigations would clearly be desirable for extrapolation to  
205 alternative design problems.

206

## 207 REFERENCES

- 208 Anderson, C., Wijewickreme, D., Ventura, C. & Mitchell, A. (2004). Full-scale laboratory  
209 testing of buried polyethylene gas distribution pipelines subject to lateral ground  
210 displacements. In *Proceedings of the 13th World Conference on Earthquake*  
211 *Engineering*.
- 212 Bilgin, Ö. & Stewart, H. E. (2009). Design guidelines for polyethylene pipe interface shear  
213 resistance. *Journal of Geotechnical and Geoenvironmental Engineering, ASCE* **135**(6):  
214 809-818.
- 215 Brachman, R. W. I., Moore, I. D. & Rowe, R. K. (2000). The design of a laboratory testing  
216 facility for evaluating the structural response of small-diameter buried pipes. *Canadian*  
217 *Geotechnical Journal* **37**(2): 281-295.
- 218 Brachman, R. W. I., Moore, I. D. & Rowe, R. K. (2001). The performance of a laboratory  
219 facility for evaluating the structural response of small diameter buried pipes. *Canadian*  
220 *Geotechnical Journal* **38**(2): 260-275.
- 221 Chapman, D. N., Fleming, P. R., Rogers, C. D. F. & Talby, R. (2007). The response of flexible  
222 pipes buried in sand to static surface stress. *Geomechanics and Geoengineering* **2**(1):  
223 17-28.
- 224 Difrancesco, L. C., Selig, E. T. & McGrath, T. J. (1994). *Laboratory testing of high density*  
225 *polyethylene drainage pipes*. Geotechnical report no. CPP93-412F, Department of Civil  
226 Engineering, University of Massachusetts, Amherst
- 227 Fioravante, V., Ghionna, V. N., Pedroni, S. & Porcino, D. (1999). A constant normal stiffness  
228 direct shear box for soil-solid interfaces tests. *Italian Geotechnical Journal* **33**(3): 7-  
229 22.
- 230 Höeg, K. (1968). Stresses against underground structural cylinders. *J. Soil Mech. Found.Div.,*  
231 *ASCE* **94**(4): 833-858.
- 232 Huber, M. & Wijewickreme, D. (2014). Response of buried district heating pipelines under  
233 relative axial movements. In *Proceedings of the 10th International Pipeline*  
234 *Conference*.
- 235 Karimian, S. A. (2006). Response of buried steel pipelines subjected to longitudinal and  
236 transverse ground movement. PhD thesis, The University of British Columbia.
- 237 Kastner, R. E. (1992). Structural performance of plastic pipe used for landfill leachate  
238 collection. MS thesis, Ohio University.
- 239 Kastner, R. E., Sargand, S. M. & Mitchell, G. F. (1993). Structural performance of PVC  
240 leachate collection pipe. In *Structural performance of pipes* (Sargand, S. M., Mitchell,  
241 G. F., and Hurd, J. O. (eds)), A.A. Balkema, Rotterdam, The Netherlands, 83-95.
- 242 Porcino, D., Fioravante, V., Ghionna, V. N. & Pedroni, S. (2003). Interface behavior of sands  
243 from constant normal stiffness direct shear tests. *Geotechnical Testing Journal* **26**(3):  
244 289-301.
- 245 Rogers, C. D. F., Fleming, P. R. & Talby, R. (1996). Use of visual methods to investigate the  
246 influence of installation procedure on pipe-soil interaction. *Transportation Research*  
247 *Record 1541, Structures, Culverts and Tunnels*: 76-84.
- 248 Sargand, S. M. (1993). Structural performance of an HDPE leachate collection pipe. In  
249 *Proceedings of the 31st Annual International Solid Waste Exposition*, 381-402.
- 250 Scarpelli, G., Sakellariadi, E. & Furlani, G. (2003). Evaluation of soil-pipeline longitudinal  
251 forces. *Rivista Italiana de Geotecnica* **4**(3): 24-41.
- 252 Sheil, B. B., Martin, C. M., Byrne, B. W., Plant, M., Williams, K. and Coyne, D. (2018). Full-  
253 scale laboratory testing of a buried pipeline in sand subjected to cyclic axial  
254 displacements. *Géotechnique* **68**(8): 684-698.

255 Talesnick, M. L., Xia, H.-W. & Moore, I. D. (2011). Earth pressure measurements of buried  
256 HDPE pipe. *Geotechnique* **61**(9): 721-732.

257 Weidlich, I. & Achmus, M. (2006). Reduction of friction forces between soil and buried district  
258 heating pipes due to cyclic axial displacements. In *Proceedings of the 10th*  
259 *International Symposium on District Heating and Cooling*.

260 Wijewickreme, D., Karimian, H. & Honegger, D. (2009). Response of buried steel pipelines  
261 subjected to relative axial soil movement. *Canadian Geotechnical Journal* **46**(7):735-  
262 752.

263 Zanzinger, H. & Gartung, E. (1995). Large-scale model tests of leachate collection pipes in  
264 landfills under heavy loads. In *Advances in underground pipeline engineering*.  
265 (Jeyapalan, J. K., and Jeyapalan, M. (eds)), New York, 114-125. American Society of  
266 Civil Engineers.

267 Zanzinger, H. & Gartung, E. (1998). HDPE-geopipes, soil–structure interaction. In  
268 *Proceedings of the 6th International Conference on Geosynthetics*, 197-200.

**Table 1** Sand properties

Property	Sand K	Beach Sand
Median particle size, $D_{50}$ (mm)	0.21	0.35
Coefficient of uniformity	1.8	3.1
Specific gravity, $G_s$	2.67	2.53
Critical state friction angle, $\phi'_{crit}$ (°)	31.1	30.9
% fines (<75 $\mu\text{m}$ )	4.5	2.5

**Table 2** Summary of samples and boundary conditions

Test	Material	Moisture content, $w$ (%)	Sand cover, $h$ (m)	Overall unit weight, $\gamma'$ ( $\text{kN/m}^3$ )	Set-up (Fig. 3)	Bag pressure (kPa)	Nominal $\sigma'_v$ at pipe crown, Eq. 1 (kPa) <sup>a</sup>
K1	Sand K	< 1	0.35	15.5	(i)	25	30
K2	Sand K	< 1	0.35	15.3	(ii)	38	30
B1	Beach Sand	< 1	0.35	15.8	(i)	25	31
B2	Beach Sand	< 1	0.35	16.0	(ii)	38	30

<sup>a</sup> pressure bag area ratios of 1 and 0.64 were adopted for set-ups (i) and (ii), respectively

**Table 3** Sequence of axial displacement cycles

Cycle set	Displacement amplitude (mm)	No. cycles
A	20	5
B	2	5
C	20	3
D	2	5
E	20	3
F	2	5
G	20	3
H	2	5
I	20	3

**Table 4** Additional sequence of axial displacement cycles appended to Test B1

Cycle set	Displacement amplitude (mm)	No. cycles	Bag pressure (kPa)	Nominal $\sigma'_v$ at pipe crown, Eq. 1 (kPa)
J	20	3	32.5	38
K	20	3	40	45.5
L	20	3	47.5	53
M	20	3	25	30.5

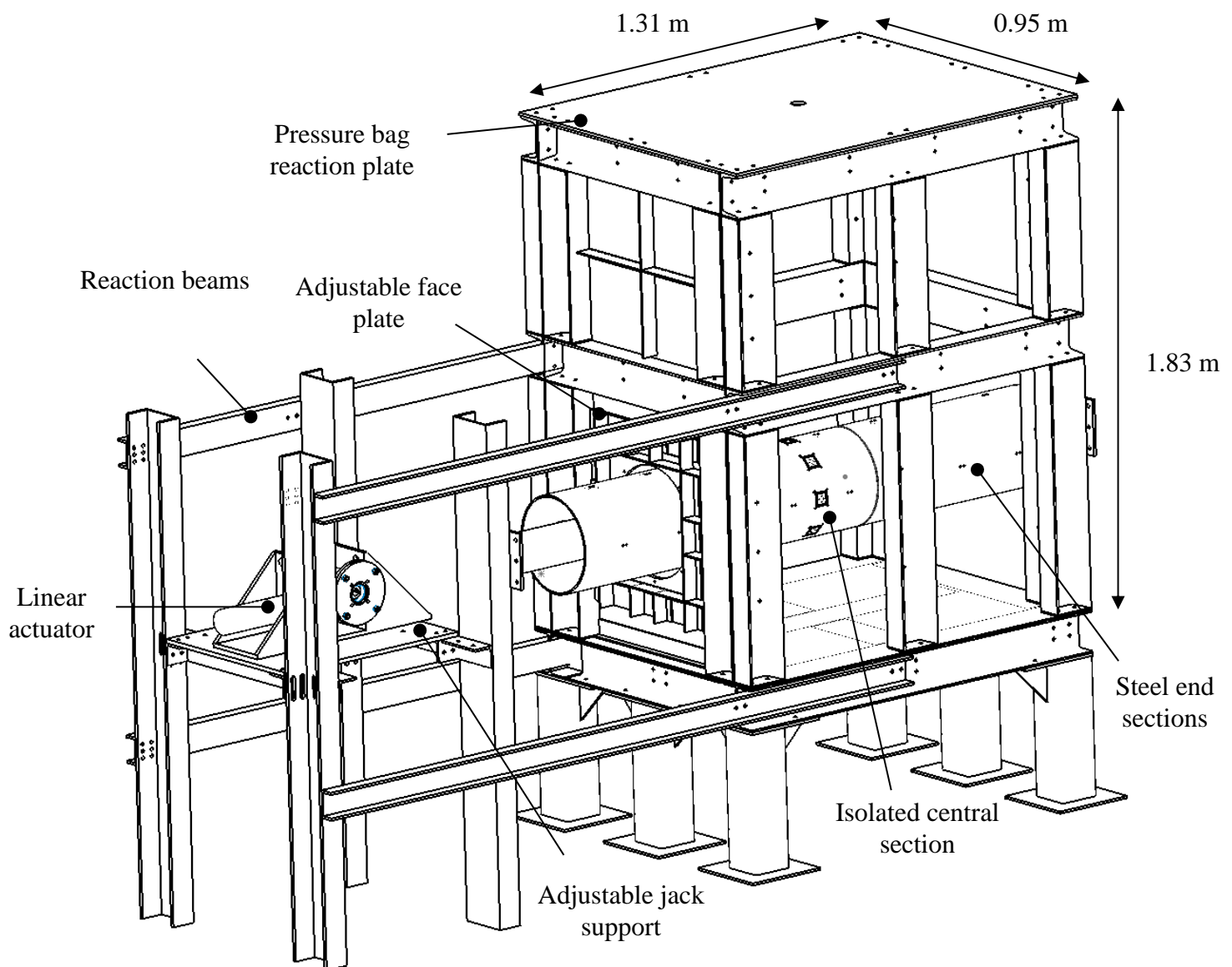


**Fig. 1** Isometric view of testing rig (tank side walls and far end plates not shown); measurements are inside dimensions of testing tank

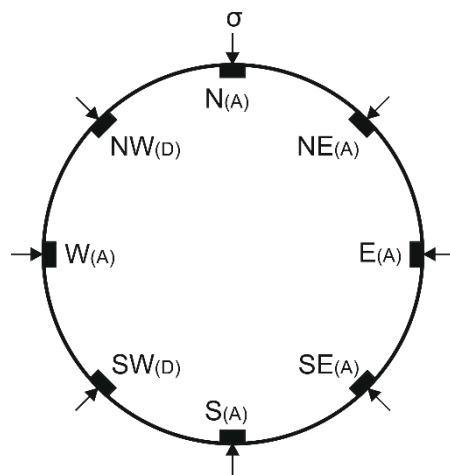


**Fig. 2** Locations of Stroud load cells (A = active cell, D = dummy cell)

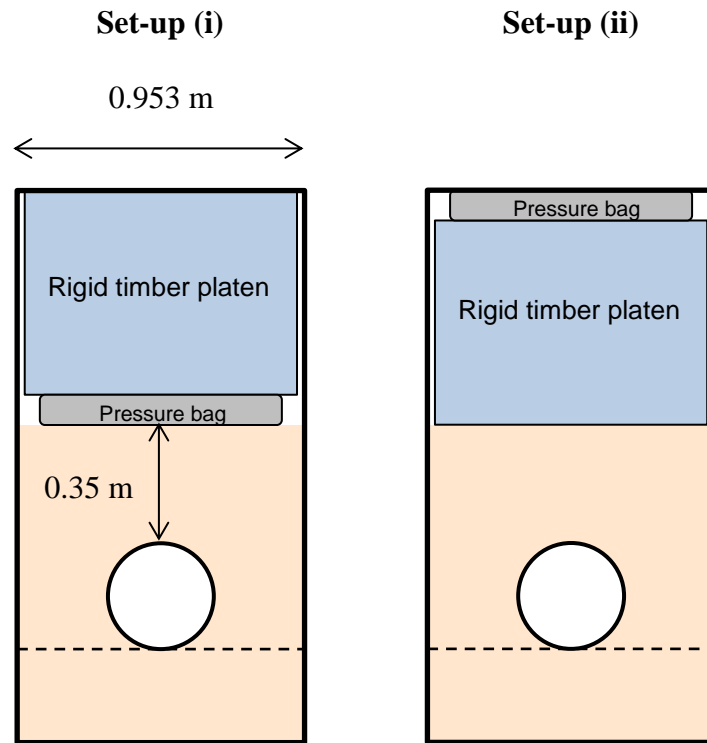


**Fig. 3** Surcharge boundary conditions adopted in the testing

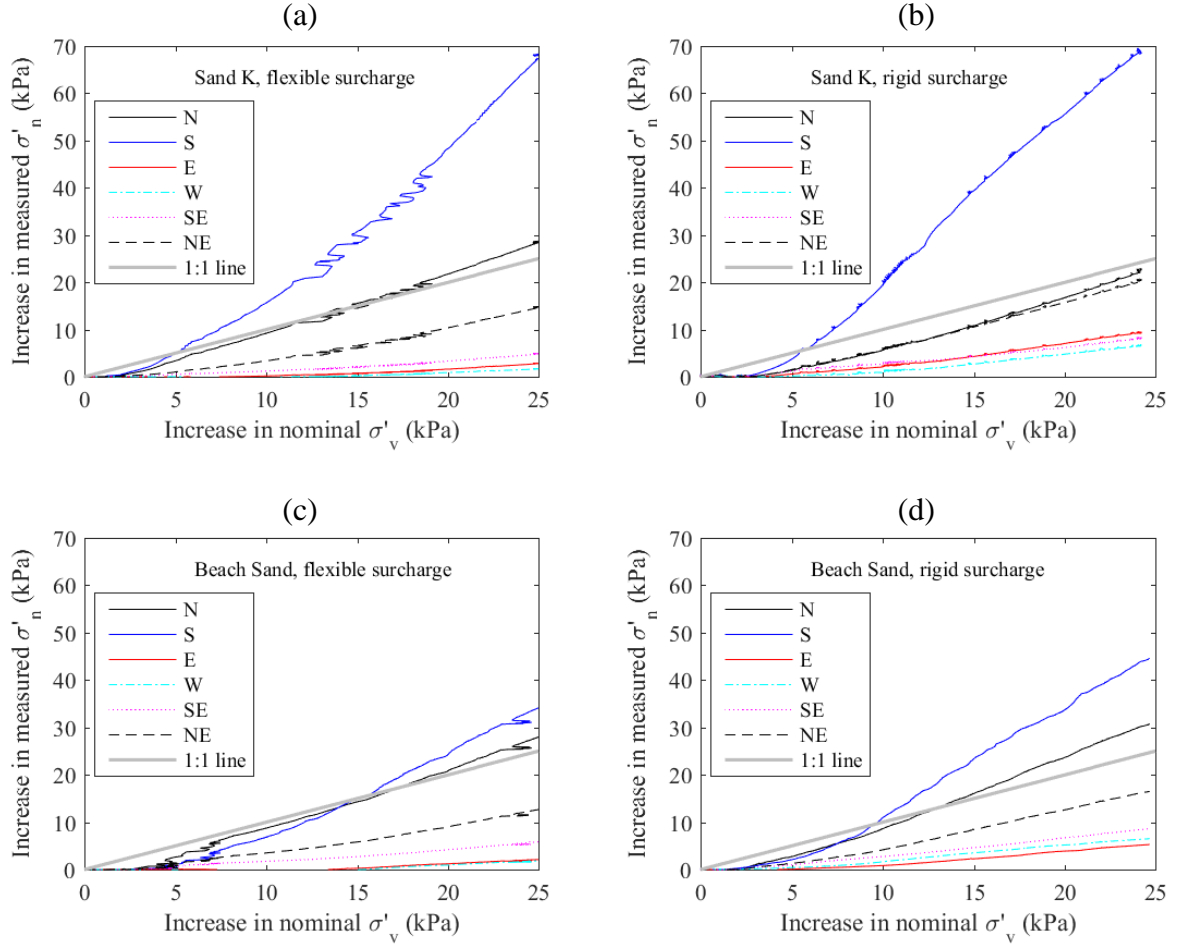


**Fig. 4** Variation in normal contact stresses during pressure bag inflation: (a) Test K1; (b) Test K2; (c) Test B1; (d) Test B2;  $\sigma'_v$  = nominal overburden pressure at pipe crown

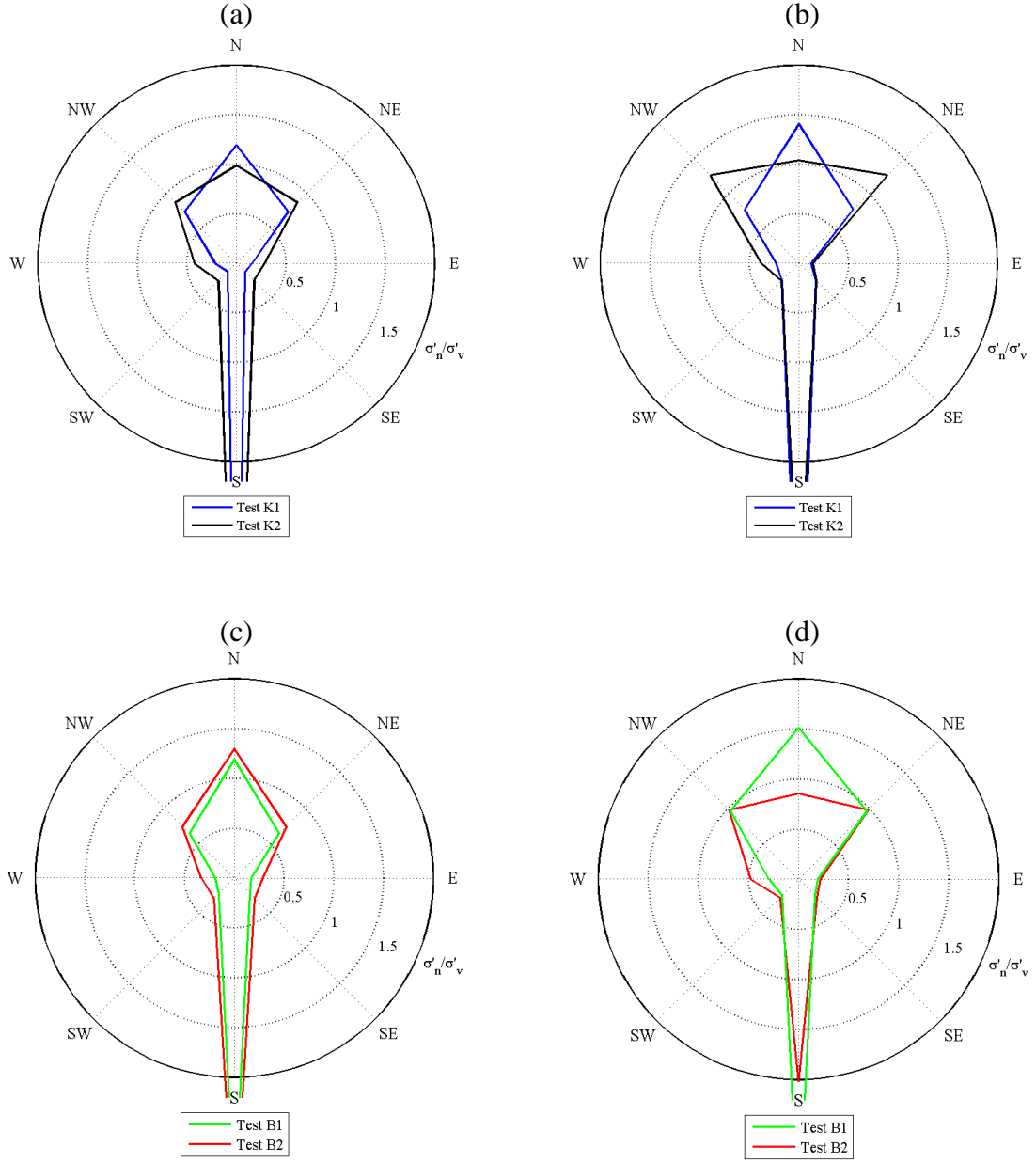


**Fig. 5** Influence of surcharge boundary condition on distribution of  $\sigma'_n / \sigma'_v$ : (a) Tests K1 and K2 initial; (b) Tests K1 and K2 final; (c) Tests B1 and B2 initial; (d) Tests B1 and B2 final;  
 $\sigma'_v$  = nominal overburden pressure at Stroud cell location

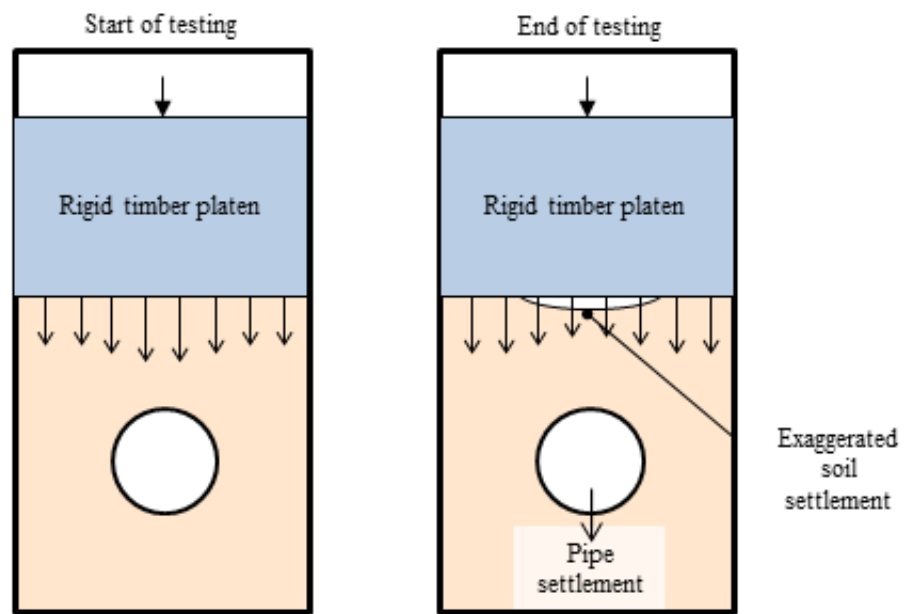


**Fig. 6** Loss of vertical pressure above pipe during cyclic axial testing with set-up (ii)

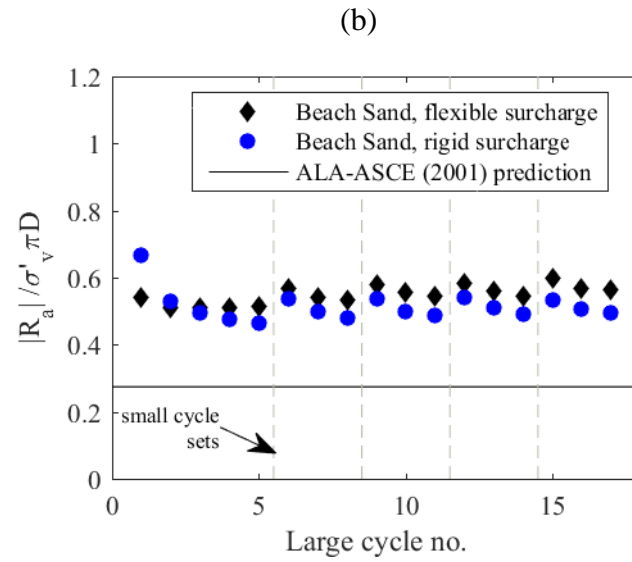
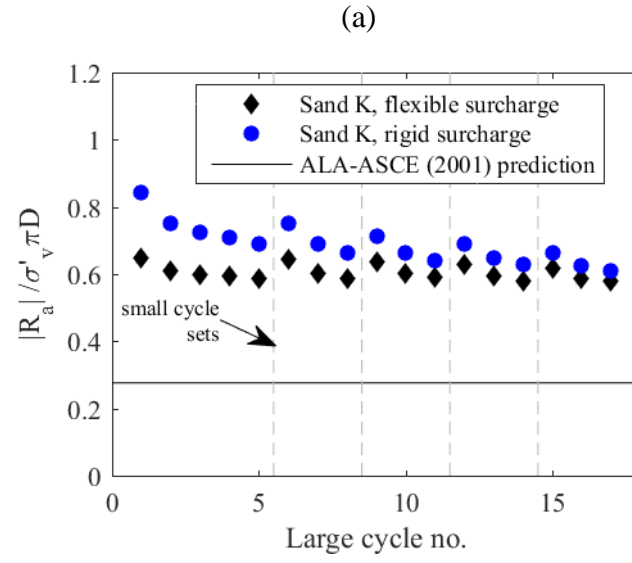


**Fig. 7** Influence of surcharge boundary condition on normalised peak axial resistance: (a) Tests K1 and K2; (b) Tests B1 and B2;  $\sigma'_v$  = nominal overburden pressure at pipe crown

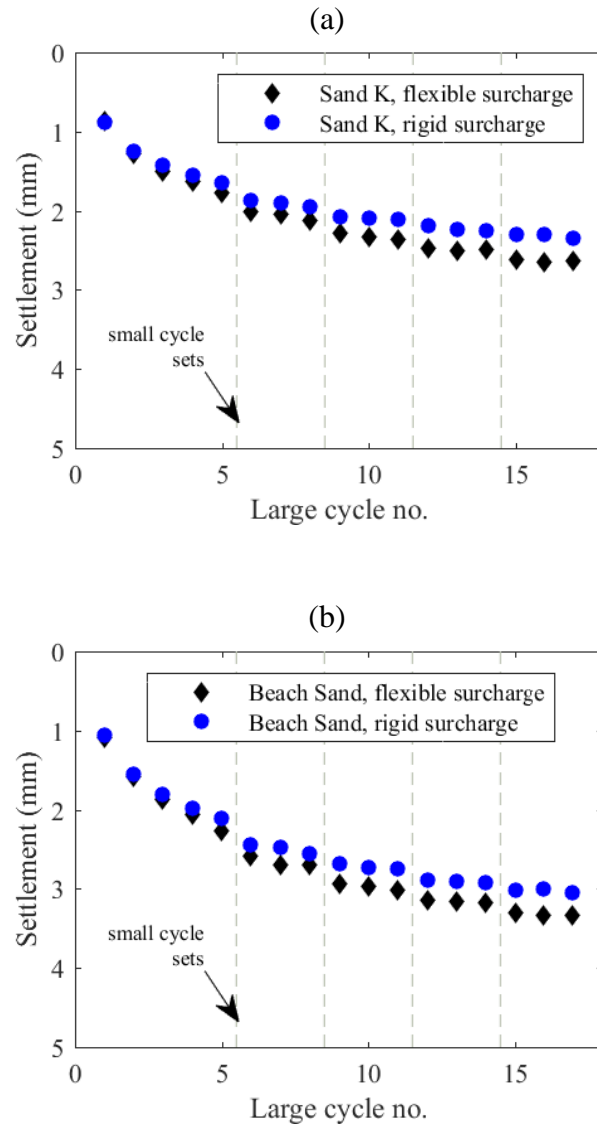


**Fig. 8** Influence of surcharge boundary condition on vertical pipe settlement: (a) Tests K1 and K2; (b) Tests B1 and B2

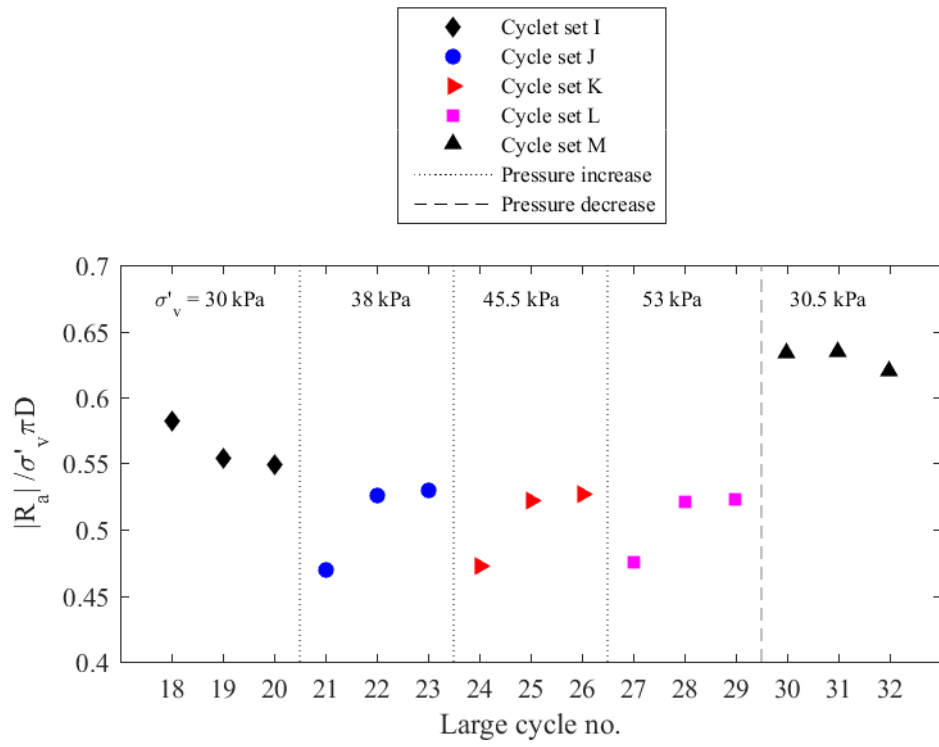


**Fig. 9** Influence of surcharge pressure on normalised peak axial resistance for Test B1 (flexible surcharge boundary condition);  $\sigma'_v$  = nominal overburden pressure at pipe crown

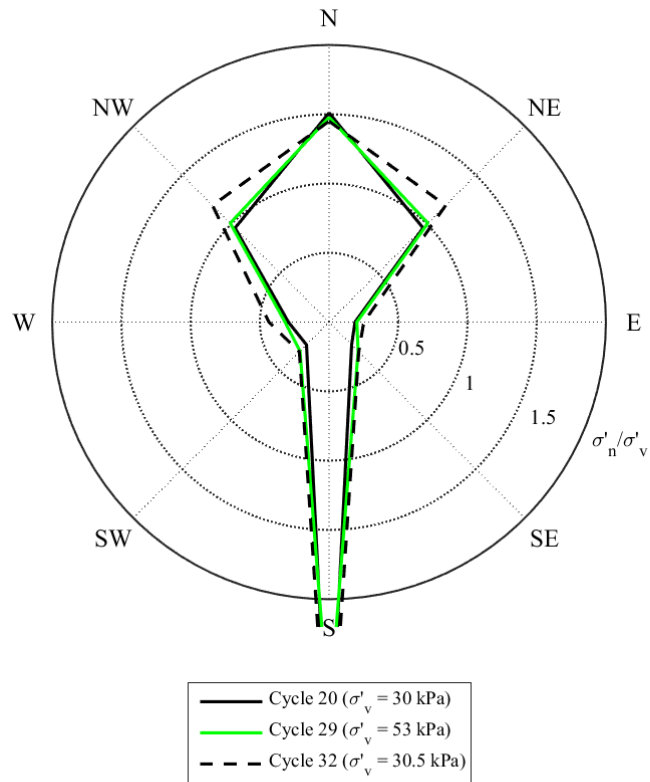


**Fig. 10** Comparison of stress distributions before and after pressure increase phases for Test B1 (flexible surcharge boundary condition);  $\sigma'_v$  = nominal overburden pressure at Stroud cell location